Article

Toxic cultures: e-cigarettes and the oral microbial exposome

Check for updates

Michelle Lee-Scott Beverly[1], Prem Prashant Chaudhary[2], Shareef Majid Dabdoub [3], Shinae Kim[4], Emmanouli Chatzakis[5], Kathryn Williamson[5], Sukirth Murthy Ganesan [3], Manoj Yadav[2], Grace Ratley[2], Brandon N. D'Souza[2], Ian A. Myles[2] & Purnima S. Kumar [1] ✉

We tested the hypothesis that e-cigarette aerosol is metabolized by the indigenous oral microbiome, leading to structural and functional alterations. We combined untargeted metabolomics of in vitro commensal-rich and pathogen-rich biofilms with metatranscriptomics and fluorescent microscopy and verified the results in human samples. Spectral deconvolution of 4215 peaks identified 969 exposomal and endogenous metabolites that mapped to 23 metabolic pathways. The metabolites clustered by both aerosol characteristics and biofilm composition; and several were verified in human saliva of vapers. E-cigarette exposure upregulated xenobiotic degradation, capsule, peptidoglycan biosynthesis, organic carbon-compound metabolism, antimicrobial resistance, and secretion systems. E-cigarette exposure also altered biofilm architecture characterized by low surface-area to biovolume ratio, high biomass, and diffusion distance. In conclusion, our data suggest that bacterial metabolism of e-cigarette aerosol triggers a quorum-sensing-regulated stress response which mediates the formation of dense, exopolysaccharide-rich biofilms in health-compatible communities and antibiotic resistance and virulence amplification in disease-associated communities.

In common with all living organisms, the human body is responsive to the surrounding environment; an ideology that led to a new field of study in 2005: Exposomal Biology[1]. The environmental exposures that humans experience over their lifetime can be either internal, specific external or general external[2]. Anthropogenic or lifestyle-based influences are examples of specific external exposures; and prominent among these are diet, tobacco, and alcohol[2].

One such exposomal factor that has become a concern in recent times is the electronic cigarette (E-cig), because of its potential to have an impact from a very early age[3]. Also known as an Electronic Nicotine Delivery System (ENDS), it is a battery-operated device that heats up a mixture of humectant, flavoring agents and/or nicotine under high pressure and temperature to create an aerosol that is then inhaled through the mouth. These devices entered the US market a little over 15 years ago and have captured a large market share within this short period of time. Indeed, the CDC reports a 46.6% increase in sales and a 46% rise in the number of brands (from 184 to 269) between January 2020 and December 2022[4]. The National Youth Tobacco Survey of 2022 found that 2.5 million school children have used these devices, most of them on a daily basis,

exponentially increasing the risk of lifetime nicotine addiction and creating a gateway to other forms of addiction[5].

Emerging studies, as summarized in the Review of the Health Effects of ENDS by the National Academies of Sciences, Engineering, and Medicine Committee[6], provide substantial evidence that e-cigarettes influence the pathophysiology of human diseases in several ways, for example, by promoting endothelial dysfunction and oxidative stress. Data from human studies also catalog the deleterious effects of e-cigarette metabolites on the cardiovascular and respiratory systems[7-9].

The oral cavity is the first point of contact, and therefore, the first organ system to be impacted by this aerosol. We have previously used metagenomics to demonstrate that e-cigarette use is associated with higher virulence signatures and a brisk proinflammatory signal in the oral cavity of clinically healthy e-cigarette users[10]. Other studies using meta-taxonomics have also demonstrated similar dysbiotic changes in subjects with periodontitis[11-13] However, the mechanisms by which e-cigarettes create this pathogen-enriched ecosystem are not known.

Man is a holobiont[14], and therefore, the exposome has to be interrogated not only through the lens of adaptive/maladaptive changes in

¹Department of Periodontics and Oral Medicine, School of Dentistry, University of Michigan, Ann Arbor, MI, USA. ²Epithelial Therapeutics Unit, National Institute of Allergy and Infectious Diseases Laboratory of Clinical Immunology and Microbiology, IH, Bethesda, MD, USA. ³Department of Periodontics, School of Dentistry, University of Iowa, Iowa City, IA, USA. ⁴Brillient Corporation, Reston, VA, USA. ⁵Department of Food Sciences, The Ohio State University, Columbus, OH, USA. ✉e-mail: kpurnima@umich.edu

1

human cells, but also by quantifying changes in the microbiomes that we host. While this is conceptually attractive, the complexity of biological systems as well as the multiplicity of exposures over the lifetime create seemingly unsurmountable challenges to unraveling these interactions. However, the advent of high-dimension biology has enhanced our ability to identify the compounds that we are exposed to and the metabolic profiles that result from these exposures. Indeed, by mapping changes at the DNA, RNA, protein, or metabolite level in response to a specific environmental exposure, it is possible to define an "exposotype" and to explicate its molecular underpinnings.

In the present study, we hypothesized that bacteria metabolize e-cigarette aerosol and that these metabolites play important roles in altering community structure, function, and topography. We aimed to test this hypothesis using a combinatorial enumeration of transcriptional events and metabolic activity, quantification of biofilm topography and verification of the in vitro findings in the human exposome.

Results

Certain chemicals identified in e-cigarette aerosol have known cytotoxic effects

We began our analysis by investigating the chemical composition of a commercial brand of tobacco-flavored nicotine-containing and nicotine-free e-cigarette aerosol using GCMS. Overall, 365 (412) compounds were detected in nicotine-free (nicotine-containing) aerosol, of which 27 (32) were duplicate peaks. 25 (36) were also identified in clean air controls and subtracted resulting in 313 and 308 compounds respectively; less than half (188) of which were common to both aerosols (Supplemental Table 1), indicating a large difference between the constituents. Notable among these common compounds were paraldehyde, acetyl chloride, allyl acetate, anabasine, dimethylphosphine, diacetyl sulphide, diglycerol, dimethyl sulfoxide, ethylhydroxylamine, erythritol, fluoro-acetic acid, glyceraldehyde, glycerin, glycol, nitro-methane, phosgene, propylene glycol, trimethylpropoxy silane, thioacetic acid, trimethylphosphine, thiodiglycol, and xylitol. Additionally, among the predominant compounds identified in nicotine-free aerosol were esters and salts of hexanoic and octanoic (caprylic acid) and propionic acid, while minor tobacco alkaloids (nornicotine, anabasine, cotinine, nicotine nitriles) and compounds containing butane and silanes were more frequently identified in nicotine-containing aerosol. Twelve of these compounds were identifiable as "dangerous chemicals" and eight were associated with 'warnings' according to the Globally Harmonized System of Classification and Labeling of Chemicals (GHS). According to the associated Material Safety Data Sheets (MSDS), 15 chemicals were labeled as harmful when ingested or inhaled at high concentrations.

Oral bacteria metabolize e-cigarette aerosol

We then investigated the metabolic byproducts produced by commensal-rich, intermediate, and pathogen-rich biofilms when exposed to these nicotine-containing or nicotine-free e-cigarette aerosols, or to clean-air (control). The three biofilm types were representative of the health-compatible communities and those associated with periodontital diseases, namely, gingivitis and periodontitis. We have previously documented the composition and architecture of these biofilms[15]. Briefly, SEM analysis revealed a multi-layered structure, fibril-mediated coaggregation between colonizers, channel-like structures separating the micro-colonies, and a sequential overlaying of the secondary colonizers (bacillary, cocco-bacillary shapes) over the primary colonizers (cocci). Compositionally, the abundances of the specific species in the biofilms were similar to those reported from in vivo biofilms in periodontal health and disease[16,17]. Time series analysis revealed that the majority of metabolites and compounds were generated within one hour of exposure to e-cigarette aerosol ($p < 0.05$, ANOSIM, Fig. 1A). Based on this and the confocal data (see relevant section below), we investigated the metabolites generated following one-hour of e-cigarette exposure using TIMS-ToF. Overall, 4474 peaks were generated and 4215 were identifiable beyond a zero threshold. 3505 remained after subtracting those identified in the clean-air and no-biofilm control groups

Of these, only 969 mapped to unique metabolites following spectral deconvolution and annotation to the molecular level. 23 pathways were mapped corresponding to these metabolites (Supplemental Table 2). During this period, commensal biofilms demonstrated an $8.2 \pm 2.6\%$ ($7.4 \pm 1.3\%$, $7.9 \pm 3.9\%$) decrease in viability when compared to pre-exposure levels, while secondary and tertiary biofilms demonstrated a $12.8 \pm 1.3\%$ ($8.9 \pm 5.3\%$, $10.4 \pm 3.9\%$) and $9.4 \pm 4.6\%$ ($11.4 \pm 5.8\%$, $8.8 \pm 3.3\%$) reduction following nicotine-free (nicotine-containing, clean-air exposure) respectively. The decrease in viability was not statistically significantly different between biofilm types or exposure type ($p > 0.05$, ANOVA).

Since metabolites can also be products of normal bacterial cell cycle, we investigated the percentage of naturally occurring metabolites versus those that are part of the human exposome (Supplemental Table 2). Over 82% of the metabolites that were identifiable to a molecular formula belonged to the category of human exposomes based on the Human Metabolite Database[18]. This category was also the most numerically abundant class of metabolites identified. 27% of the exposome family of compounds probabilistically mapped to antimic, anti-fungal and anti-bacterial agents (Supplemental Table 2) based on the Lotus database (https://lotus.naturalproducts.net/).

Interestingly, the predominant bacterial metabolites were quorum-sensing molecules and dipeptides, pointing to significant communications among the gram-positive and gram-negative bacteria in the multi-species biofilms.

To gain insights into the sources of variability in the e-cigarette metabolome, we used principal components analysis (PCA) on variance-stabilized abundances of peaks. PCA revealed both nicotine concentration (0 mg versus 6 mg) and biofilm diversity as sources of variation, creating 6 distinct clusters ($p = 0.008$, ANOSIM, Fig. 1B). However, the Chao and Shannon indices demonstrated the greatest level of metabolite diversity when all biofilms were exposed to e-cigarette aerosol versus clean air ($p = 0.012$, Wilcoxon signed rank test, Fig. 1C, D), but the differences were not significant based on biofilm type. Furthermore, although enrichment analysis identified 879 metabolites common to both nicotine-free and nicotine-containing aerosol (Supplemental Table 2), DESeq revealed statistically significant differences in abundances between 95 of these common metabolites ($p < 0.05$, FDR adjusted Wald Test, Supplemental Table 3). Moreover, 887 metabolites were unique to nicotine-containing aerosol and 1027 metabolites were unique to nicotine-free aerosol.

Byproducts of e-cigarette metabolism depend on bacterial community composition

Univariate analysis of nicotine-free and nicotine plus aerosol using partial least squares discriminant analysis (PLSDA) demonstrated that 39.1% of the variation between biofilms was explained by component 1 following exposure to nicotine-free ENDS ($Q^2 = 0.75525$, $R^2 = 0.80226$), while exposure to nicotine-containing vapor accounted for 37.6% of the variation of component 1 ($Q^2 = 0.73132$, $R^2 = 0.79832$, Fig. 2A, B). indicating that biofilm diversity was also a robust determinant of metabolite profile. A machine-learning algorithm trained on the metabolite profiles identified 15 compounds as discriminants of biofilm composition and vapor type (Fig. 2C). Covariate analysis using two-way ANOVA demonstrated a significant difference in 13 metabolites based on biofilm exposure alone, 17 metabolites for ENDS exposure alone, and 17 metabolites for the interaction between biofilm and ENDS exposures ($p < 0.05$, ANOVA, Fig. 2D and Supplemental Table 2). Additionally, spectral deconvolution revealed that 423 metabolites were generated from nicotine-free aerosol when exposed to commensal-rich biofilms, while intermediate biofilms generated 505 metabolites and pathogen-rich generated 566 (Supplemental Table 2). Similarly, following exposure to nicotine-containing aerosol, 380, 436, and 597 compounds were generated by commensal-rich, intermediate, and pathogen-rich biofilms. Pathogen-rich biofilms were exposed to nicotine-containing aerosol generated significantly greater amounts of compounds related to the pyridine and pyrrolidine pathways of nicotine metabolism (notably, 2-ketoglutaramate, 6-hydroxy-N-methylmyosmine, and ethyl 4-
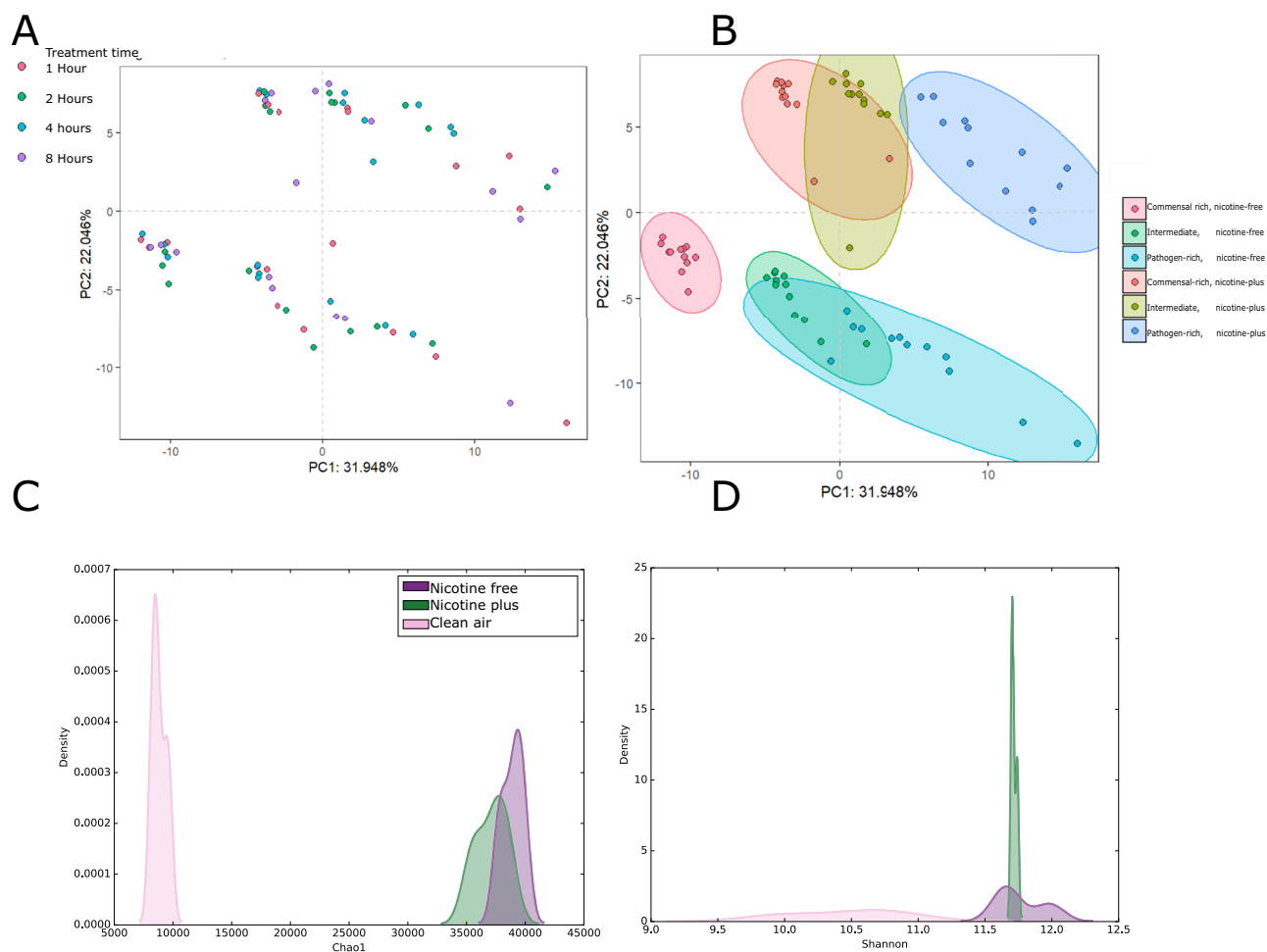
Fig. 1 | Metabolite diversity and generation time. Principal Components analysis (PCA) of the metabolites generated over 8 h are shown in (**A**). Data was acquired through untargeted one-dimensional (1D) 1H NMR and each bucketed region was normalized to the total sum of the spectral intensities prior to analysis. All samples were run in triplicates, and the experiments were duplicated. Only peaks that exceeded the zero threshold were inducted into analysis. The majority of the metabolites were generated within one hour of exposure to e-cigarette vapor ($p = 0.008$, ANOSIM). PCA also revealed nicotine concentration (0 mg versus 6 mg) and biofilm diversity as sources of variation along with (**B**). Kernel density plots of Chao and Shannon indices (**C**, **D** respectively) demonstrated the significant differences based on type of aerosol ($p = 0.012$, Wilcoxon signed rank test).

(acetylthio)butyrate) than commensal-rich biofilms. A machine learning algorithm trained on this dataset was able to predict e-cigarette exposure with 94% sensitivity and 92% specificity, and biofilm diversity with 82% sensitivity and 76% specificity. It also identified 15 compounds that were able to discriminate between biofilm diversity and aerosol composition (Fig. 2C). Notable among these were homo-serine-lactone, pyrollidine and dopamine, which showed high out-of-box (OOB) prediction for nicotine-containing aerosol and pathogen-rich biofilms.

Metabolite enrichment analysis corroborated our findings that pathways regulated by these metabolites depend on biofilm diversity. For instance, the compounds generated from nicotine-free and nicotine-containing aerosol by commensal biofilms mapped to significantly fewer metabolic pathways when compared to those produced by intermediate and pathogen-rich biofilms (Fig. 3A–I and supplemental Table 2). Globally, commensal-rich biofilms were significantly enriched in pathways of lipid, carbohydrate, and energy metabolism, xenobiotic degradation, and intermediate metabolites. E-cig metabolism by intermediary biofilms impacted metabolism of nucleotides, beta-alanine, caffeine, riboflavin, tyrosine, vancomycin, alanine, carbohydrate (fructose, galactose, ketone bodies), lipid, and proteins, steroid biosynthesis, and glycan biosynthesis and degradation. Pathogen-rich biofilm metabolism demonstrated enrichment of pathways related to biosynthesis of flavenoids, indoles, ascorbates, ketones, proteo-glycans, steroid, inositol and pyridine alkaloids, and the

pyrrolidine pathway, among others. Of note, several oligopeptide metabolites were also enriched, pointing to enrichment of proteolysis-related pathways. However, lack of a peptide pathway database precluded their inclusion into the pathway mapping.

E-cigarettes induce quorum-sensing regulated gene expression in oral biofilms

Since several peaks identified in the study mapped to bacterial quorum sensing molecules; and compounds and metabolites such as glycerol, acetaldehydes, glycol etc. are known to impact bacterial growth and development, we investigated gene expression profiles in commensal-rich, intermediate, and pathogen-rich biofilms following one hour of exposure to nicotine-containing and nicotine-free aerosol and compared them to clean-air exposure (Fig. 4A and Supplemental Table 4). 86 million analyzable sequences passed quality checks and were available for analysis. The number of sequences per sample ranged from 1.02 to 2.3 million, and did not demonstrate statistically significant differences based on biofilm or exposure type. These sequences mapped to 8973 transcripts. Multivariable association analysis identified 2049 KEGG orthologs that were significantly upregulated following exposure to nicotine-free or nicotine-plus aerosol when compared to clean-air (Supplemental Table 4). 1872 of these were significantly upregulated in response to nicotine-plus aerosol exposure when compared to clean air,
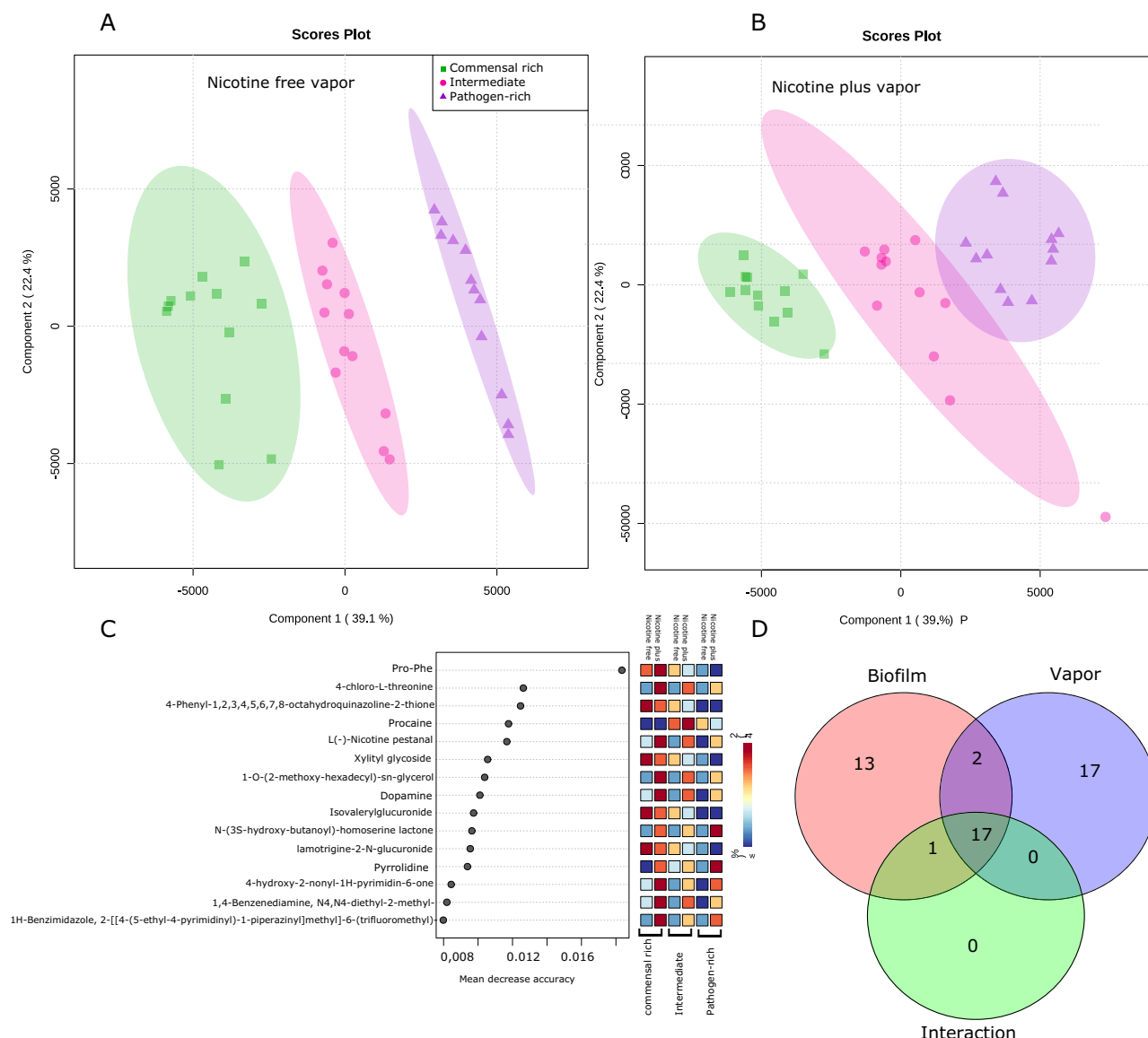
Fig. 2 | Microbial community composition is also a determinant of metabolite profiles. Univariate analysis of nicotine-free and nicotine plus aerosol using partial least squares discriminant analysis (PLSDA) demonstrated that 39.1% of the variation between biofilms was explained by component 1 following exposure to nicotine-free ENDS ($Q^2 = 0.75525$, $R^2 = 0.80226$), while exposure to nicotine-containing vapor accounted for 37.6% of the variation of component 1 ($Q^2 = 0.73132$, $R^2 = 0.79832$, **A**, **B**). indicating that biofilm diversity was also a robust determinant of metabolite profile. A machine-learning algorithm trained on the metabolite profiles identified 15 compounds as discriminants of biofilm composition and vapor type (**C**). Covariate analysis using two-way ANOVA demonstrated a significant difference in 13 metabolites based on biofilm exposure alone, 17 metabolites for ENDS exposure alone, and 17 metabolites for the interaction between biofilm and ENDS exposures ($p < 0.05$, ANOVA, **D**). All samples were run in triplicates, and the experiments were duplicated. Only peaks that exceeded the zero threshold were inducted into analysis. Data supporting this figure can be found in Supplemental File 2.

and 2257 in response to nicotine-free aerosol. Interestingly, 1810 of these genes were upregulated in response to both nicotine-free and nicotine-rich aerosol, of which, 783 belonged to the core guild of genes (see methods for definition). Over 100 of these core transcripts encoded quorum sensing and competence, 37 coded for biofilm formation and 72 genes contributed to glycerol metabolism. Among the 1810 genes, 62 were unique to nicotine-plus aerosol, and 457 unique to nicotine-free e-cigarette vapor. Again, when these unique gene sets were probed for quorum sensing, biofilm and glycerol metabolism, 10 (15), 7 (21), 10 (18) encoded for these functions following nicotine-free (nicotine-plus) exposure. When the analyses were directed to biofilm type, 458 and 475 genes were significantly overexpressed in intermediate and pathogen-rich biofilms when compared to commensal-rich biofilms respectively. Prominent among the genes upregulated in intermediate and pathogen-rich biofilms were those encoding organic carbon-compound metabolism, quorum sensing, antimicrobial resistance, secretion systems and transporters. Commensal-rich biofilms demonstrated upregulation of genes encoding capsule, peptidoglycan and glycosaminoglycan biosynthesis, rhamnose containing glycans, and extracellular polysaccharide biosynthesis, notably sialic acids, e.g., legionaminic acid and neuraminic acid. Moreover, graph theoretics revealed robust and statistically significant correlations between transcripts and metabolites (Fig. 4B–G). In commensal-rich biofilms, two large hubs demonstrating high betweenness and degree centrality were evident, one that was anchored by genes encoding phosphotransferase systems, transporters (carbohydrate, oligopepetide) and metabolites corresponding to lipid, carbohydrate, and energy metabolism. Prominent anchors of the second large network were genes that corresponded to xenobiotic degradation, and stress response and metabolites that mapped to the xenobiotic degradation pathway. Pathogen-rich
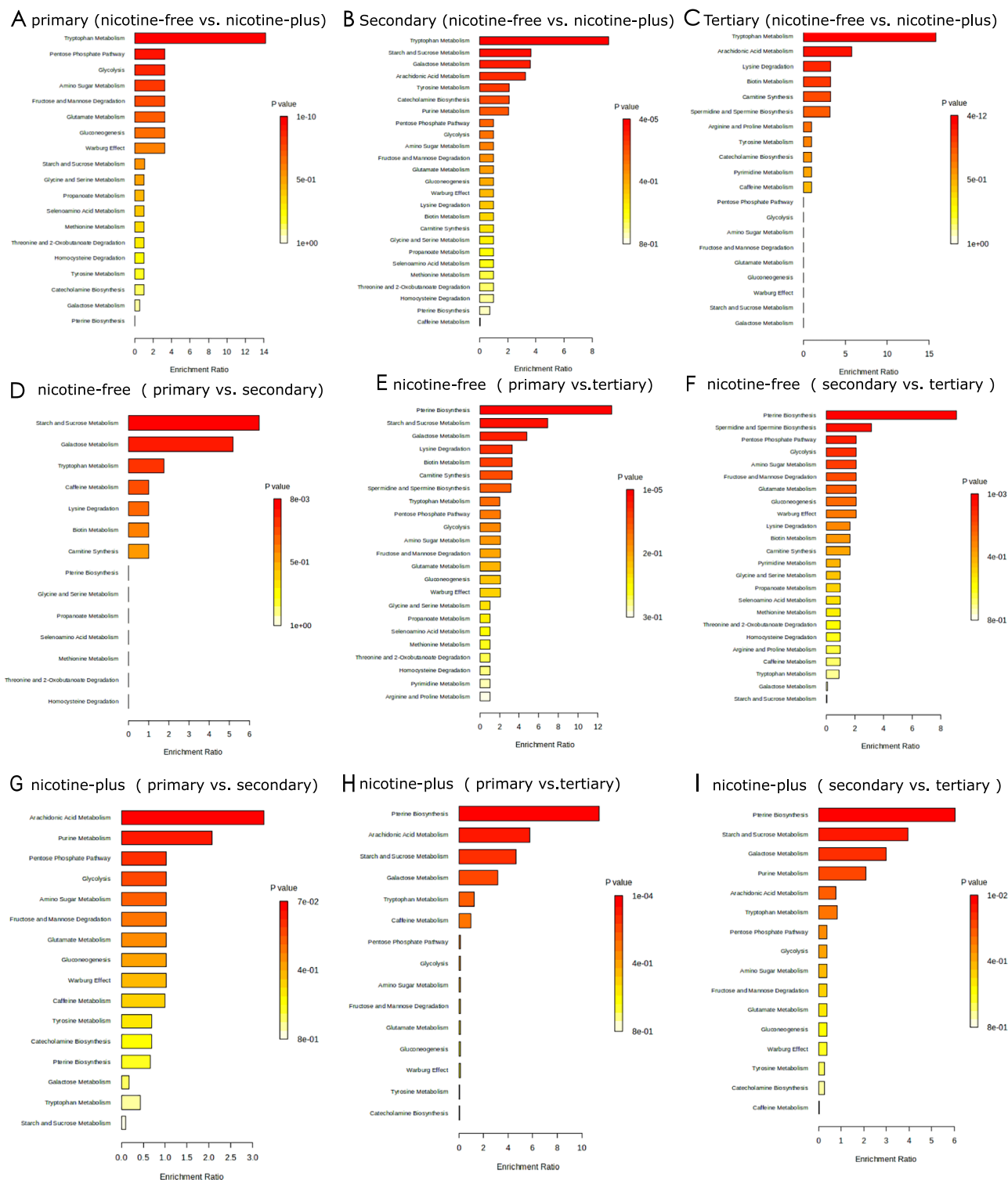
Fig. 3 | Pathway enrichment analysis identifies key biological functions impacted by vapor exposure. A–C compares pathways that are upregulated in commensal-rich, intermediate, and pathogen-rich communities following exposure to nicotine-free and nicotine plus e-cigarette vapor. **D–F** compares the pathways upregulated in the three biofilms by nicotine-free vapor and **G–I** compares the pathways upregulated in the three biofilms by nicotine-plus vapor. All samples were run in triplicates, and the experiments were duplicated. Only peaks that exceeded the zero threshold were inducted into analysis.

networks also demonstrated two large hubs, however, the hubs evidenced one-third (one-fourth) fewer connectivity between metabolites and transcripts than commensal-rich (intermediate) biofilms, as well as one-tenth (one-twelfth) betweenness centrality than commensal-rich (intermediate) biofilms. One hub consisted of networks between quorum sensing and bacterial motility genes with metabolites related to ketone and steroid biosynthesis, while bacterial metabolites related to quorum sensing correlated with genes encoding antimicrobial resistance, siderophores, osmotic stress, molecular chaperones and CRISPR in the second network neighborhood.
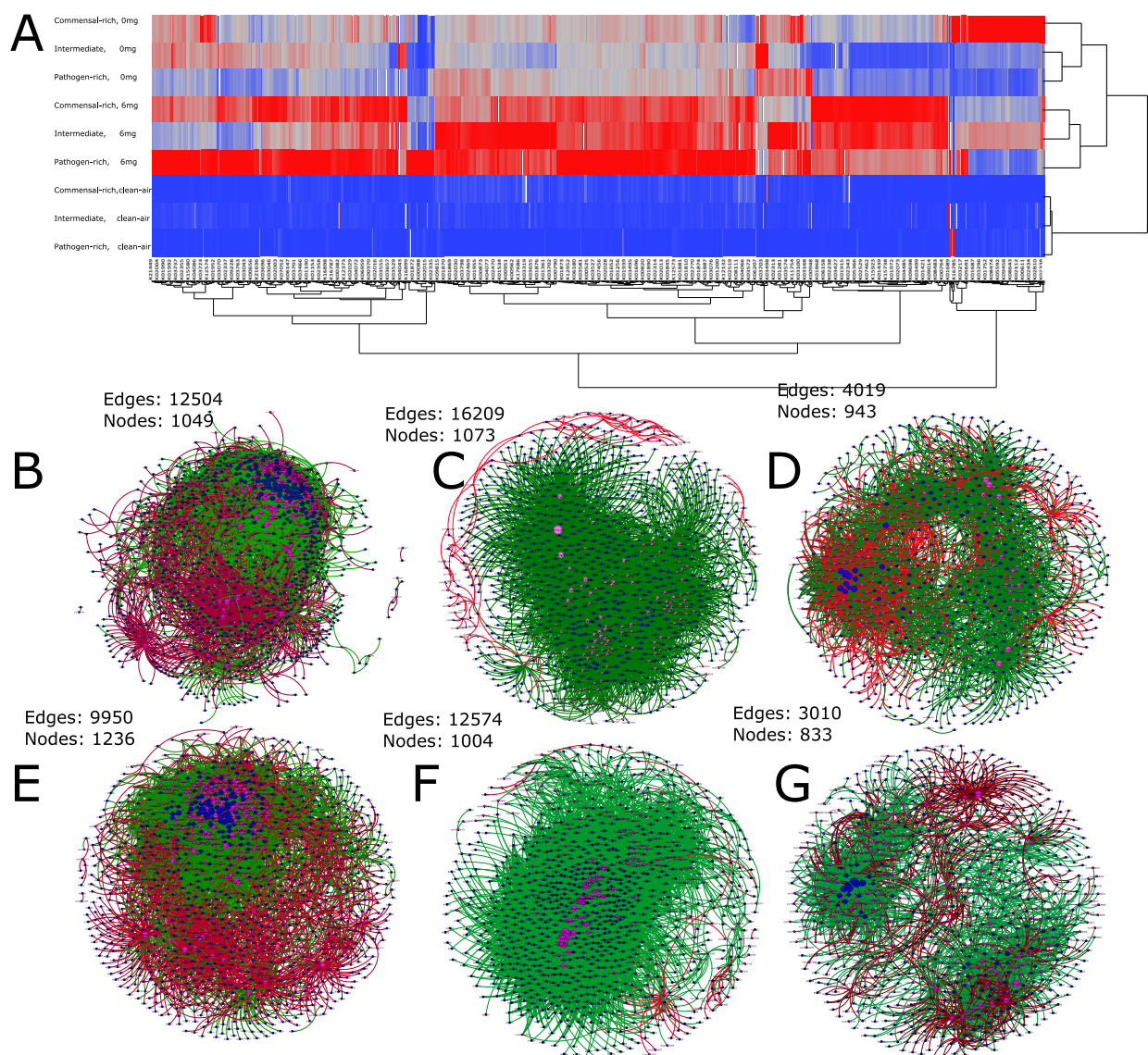
Fig. 4 | E-cigarettes induce quorum-sensing regulated gene expression in oral biofilms. Heatmap of KEGG orthologs that were upregulated following exposure to nicotine-free or nicotine plus vapor or clean-air is shown in (**A**). All samples were run in triplicates, and the experiments were duplicated. Data supporting (**A**) can be found in Supplemental Table 4. Co-occurrence networks between metabolites and microbial transcripts in each group are shown in (**B–G**). Commensal-rich biofilms are shown in (**B, E**), Intermediate in (**C, F**), and pathogen-rich in (**D, G**). Nicotine-free vapor exposure is represented in (**B–D**) and nicotine-plus vapor exposure is shown in (**E–G**). Each network graph contains nodes (circles) and edges (lines). Nodes represent metabolites (pink) and KEGG-annotated transcripts (blue), and edges represent Spearman's rho. Edges are colored green for positive correlation and red for negative correlation. Only significant correlations ($P < 0.05$, t test) with a coefficient of at least 0.80 are shown.

E-cigarette exposure alters biofilm topography

To explore the structural impact of these metabolic and transcriptional changes, we used confocal laser scanning microscopy to visualize the biofilms and computed topographical parameters with IMARIS. Exposure to nicotine-free and nicotine-plus aerosol increased the surface area of the biofilms within one hour of exposure, followed by a steady decline over 8 hours (Fig. 5d(i), (ii)). For further experiments, we selected the 1-h biofilm. Several topological features provided evidence of adaptation of biofilm to the environment even after a short period of exposure to aerosol (Fig. 5e(i–iv)). The most salient feature was the significantly higher surface-to-volume ratio in aerosol-conditioned commensal-rich biofilms when compared to clean air control. In further confirmation of this, this difference in ratios was evident only in the live cells (Fig. 5e(i)), not in the dead cells (Fig. 5e(ii)), suggesting a dynamic rearrangement of growth patterns. More importantly, the average biomass (mass that is connected to the base or substratum,

(Fig. 5e(iii)) and diffusion distances (Fig. 5e(iv)) were also significantly higher based on vaping exposure in commensal-rich communities.

Salivary metabolome profile of e-cigarette users recapitulates metabolism of nicotine-plus aerosol by pathogen-rich biofilms

We then investigated whether these metabolites could be identified in the saliva of a previously characterized cohort of e-cigarette users, dual users of e-cigarettes and cigarettes, and former smokers who currently use e-cigarettes[10]. We identified 3645 metabolites and compounds beyond a zero threshold. Spectral deconvolution and annotation to the molecular level identified 513 unique metabolites. As expected, psLDA revealed significant separation between the metabolomic profiles of pure e-cigarette users when compared to dual and former smokers. (Fig. 6 and Supplemental Table 5). We then compared these metabolome profiles with those generated by in vitro biofilms 196 of these were also identified in the in vitro analysis (Supplemental Table 5).
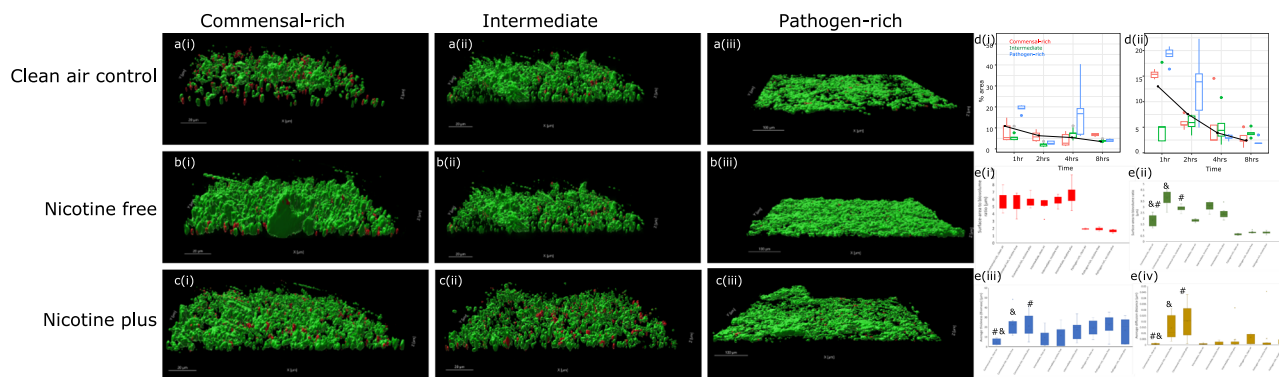
Fig. 5 | E-cigarette exposure alters biofilm topography. Representative confocal images (selected randomly from those used in the analysis) of commensal-rich biofilms consisting of *S. oralis*, *S. sanguis*, *S. mitis*, *A. naeslundii*, *N. mucosa*, and *V. parvula*, intermediate biofilms (including intermediate colonizer (*F. nucleatum*) to the aforementioned species) and pathogen-rich biofilms (intermediate biofilms that were further colonized by *P. gingivalis*, *F. alocis*, *Selenomas sputigena*, *S. noxia*, *C. gracilis*, *P. intermedia*, *P. micra*, and *T. forsythia*) following exposure to nicotine-free or nicotine-plus to e-cigarette vapor and clean air controls are shown in **a(i–iii)**, **b(i–iii)**, **c(i–iii)**. The change in biofilm area following exposure to nicotine-free and nicotine-plus vapor over 8 h are shown in **d(i, ii)** respectively. Surface area to bio-volume ratio of dead and live cells are shown in **e(i, ii)** respectively, average biomass in **e(iii)** and diffusion distance in **e(iv)**. Biofilms were visualized using confocal laser scanning microscopy in (B), and surface area and volume were computed with IMARIS. In all figures, groups connected by the same symbol are significantly different ($P < 0.001$, Dunn's test with joint ranks).

Fig. 6 | Salivary metabolome profiles of e-cigarette users recapitulate metabolism of nicotine-plus vapor by pathogen-rich biofilms. Partial least squares discriminant analysis (PLSDA) revealed significant separation between the metabolomic profiles of pure e-cigarette users when compared to dual and former smokers (Q2 = 0. 45781, R2 = 0. 51411).

Discussion

In the present investigation, we integrated metabolomics (a catalog of the complex chemical reactions elicited by a perturbation) and metatranscriptomics (a repository of all genes expressed by a community in response to a particular stressor), with topographical analysis of in vitro microcosm communities and validated the findings on human samples. By doing so, we obtained a real-time readout of changes in molecular pathways and biological functions following e-cigarette exposure and found evidence to support our hypothesis that oral bacteria metabolize e-cigarette aerosols into diverse compounds and that these compounds alter the geophysiology of oral microbial ecosystems.

While several studies in the literature have used single species biofilms or planktonic bacteria for exposomal studies[19–21], we used three prototypical, well-validated microcosm communities to mimic health-compatible and

disease-associated oral microbiomes, since bacteria exist in nature in multi-species colonial relationships. It is well established that species belonging to the genera *Streptococcus*, *Veillonella*, *Neisseria* and *Actinomyces* are early colonizers and predominate in a health-compatible microbiome, and that this community increases in diversity through the bridging function mediated by *F.nucleatum*[22,23]. Periodontitis is associated with a very diverse and heterogenous community that comprises species belonging to *Seleno-monas*, *Prevotella*, *Porphyromonas*, *Filifactor*, *Parvimonas* and *Tannerella* among others. We have previously used such microcosms to investigate the impact of smoking[15] and vaping[10]. Such an approach enabled us to identify the various tactics employed by bacteria to adapt to a change in environmental conditions.

While many of the metabolites in the present investigation are unknown and uncharacterized at the present time, a group of metabolites were identified as pesticides, fungicides, miticides and anti-bacterial agents, presumably from tobacco agriculture and agents used as preservatives in the e-cigarette liquid. These compounds were appreciably more abundant in commensal-rich biofilms; and mapped to the xenobiotic degradation pathway. Corroborating this, the metatranscriptome of commensal-rich biofilms demonstrated 2–7-fold overexpression of genes belonging to this functional family when compared to intermediate or pathogen-rich biofilms. Studies on the gut microbiome demonstrate that the indigenous bacteria respond to pesticide-like chemicals by upregulating pathways of xenobiotic degradation[24], and that these altered bacterial metabolites create a proinflammatory response and modulate the permeability of the mucosal barrier[25,26]. Most importantly, several of these metabolites were also identified in the salivary metabolome of 75 disease-naïve current, former or never smokers who used e-cigarettes. Taken together, these provide a plausible biological mechanism for the exaggerated gingival inflammation that has been reported in e-cigarette users[27,28], and deserves further investigation.

Another key finding was that e-cigarettes elicit a florid quorum sensing (QS) mediated response in all oral microbial communities. The first line of evidence was the detection of homoserine lactone and dipeptides in the metabolome of all three microcosms following exposure to nicotine-free and nicotine-plus aerosol, but not clean-air. The second was that these molecules were verified in the human salivary metabolome, confirming that these in vitro findings recapitulate real life events. The third line of evidence came from the upregulation of genes encoding QS functions in the meta-transcriptome of all three biofilms; and from graph theoretics, which demonstrated robust and positive network hubs between QS molecules in the metabolome and several QS-regulated genes in the metatranscriptome. The fourth line of evidence came from the topological alterations in the biofilm architecture, where pronounced alterations were evident in the commensal-rich biofilm landscape, and to a lesser extent, in the intermediate biofilms. An important aspect of this finding was that both nicotine-free and nicotine-plus aerosols activated QS-responsive systems. While it is known that nicotine stimulates QS in bacterial biofilms[29], we now demonstrate that other components of e-cigarettes are equally efficient in eliciting this response. This finding introduces a cautionary note to the perception that nicotine-free e-cigarettes are safer than nicotine-containing aerosol.

Although the aerosol metabolites produced by commensal-rich biofilms differed based on the presence or absence of nicotine, these biofilms responded to both types of e-cigarettes by increased secretion of public goods. This was supported by the following findings: (a) The prominent QS-regulated functions in the metatranscriptome were those contributing to cell wall and capsular biosynthesis and extracellular polysaccharides. (b) Robust correlations between these transcripts and compounds corresponding to carbohydrate metabolism. (c) Topographical features indicative of poor access to resources, and evidence of geomorphological restructuring to optimize access to nutrients[30]. It is very interesting to note, in this context, that an earlier study using single-species biofilms by Catala-Valentin[31] made similar observations regarding the disproportionate effect of e-cigarettes on commensal bacteria (*Streptococcus gordonii* and *S. sanguinis*) when

compared to the caries-associated pathogen, *S. mutans*. *S. sanguinis* was a member of the biofilms that we constructed for the present study.

Public goods are extracellular secretions that are produced in response to QS-regulated stress response, the most notable among which are exo-polysaccharides, toxins, surfactants, and extracellular enzymes[32]. Since these goods are readily shared among community members, it enables diversification of the community to include 'cheaters', that is, organisms that do not produce the goods, but benefit from it. This might explain previous discoveries that the oral microbiome of e-cigarette users is distinctly more diverse and includes more species than those of non-vapers[10–13,28]. However, the production of publicly shared goods leaves the producer vulnerable to invasion and take-over by the cheaters. One strategy employed by the cooperators is to modify the spatial structure of the biofilm to partition resources and limit diffusion[33]. This is borne out by increase in surface area to biovolume ratio and large diffusion distance in commensal-rich biofilms. Bacteria increase surface to volume ratio in order to optimize access to the limited supply of nutrients. Together, the metabolomic, metatranscriptomic and topography suggest that health-compatible microbiomes that are exposed to nicotine-free or nicotine-containing e-cigarette aerosol protect themselves from stress by producing extracellular matrix and protect this exoproduct from exploitation by spatial restructuring. This possible mechanism provides a biological underpinning for recent reports of increased caries prevalence in these individuals[34–36].

QS-signaling can also induce bacteria to produce private goods, which are cytoplasmic or surface-attached proteins or metabolites[37]. Pathogen-rich biofilms demonstrated upregulation of private goods (antimicrobial resistance, histidine kinases, metal transport), as well as siderophores, which have both public and private benefits. These correlated with the pyridine and pyrrolidine pathways of nicotine metabolism by this biofilm and suggest that pathogen-rich biofilms are influenced by different elements of the aerosol than commensal-rich biofilms. This provides an explanation for the increased antimicrobial resistance that has been reported in e-cigarette users[38,39], and highlights the potential risk for failure of antimicrobial therapy in these individuals. Interestingly, the pathogen-rich biofilm landscape did not change following e-cigarette exposure, indicating that mechanisms of QS-mediated stress response differ widely between health-compatible and disease-associated communities.

In summary, within the limitations of an in vitro biofilm model and a cross-sectional human study, we demonstrate that oral bacteria vigorously metabolize e-cigarette aerosol to generate multiple compounds and chemicals. The resultant metabolome depends on the e-cigarette aerosol as well as the denizens of the bacterial biofilm. We also demonstrate that bacteria utilize QS-regulated pathways to adapt and survive e-cigarette induced stress. These survival mechanisms vary based on the microbial denizens but are similar between nicotine-free and nicotine-containing aerosol, implicating the glycerol/glycol humectant as a driver of the microbial exposotype. Importantly, we find that xenobiotic degradation by health-compatible, commensal-rich biofilms has the potential to detrimentally impact the host-microbial interface. Further studies that interrogate metabolic and transcriptional events at the host-microbial interface are urgently needed to further explicate the mechanisms by which these products create at-risk-for-harm environments.

Methods
Aerosol generation and analysis via gas chromatography-mass spectrometry (GCMS)
E-cigarette aerosol was captured for GCMS analysis by connecting a 50 mL glass syringe (Micro-mate) to the e-cigarette mouthpiece of a moderate sized vape pen with 0.2 Ω resistance coil and 3000 mAh/80 W battery. Aerosol was generated and captured following a previously described protocol by researchers at the ADA Foundation Volpe Research Center (Gaithersburg, MD) consisting of a custom acrylonitrile butadiene styrene (ABS) enclosure with a 510 adapter, precision wattage meter and power analyzer[40]. 100 mL of e-cigarette aerosol was generated based on a previously published physio-logic puffing profile (3 s puff duration, 18 s interval, repeated for 32 puffs)[41]

and immediately injected into a 22 mL GC headspace vial with polytetrafluoroethylene (PTFE)/silicone rubber septa (Perkin Elmer) using an 18-gauge needle. 1 cm^3 GC glass wool (Sigma Aldrich 20384) was used as a filter between the mouthpiece and syringe tip. Analysis was conducted using the PerkinElmer Clarus 680 Gas Chromatograph and Clarus SQ 8 C Mass Spectrometer, equipped with a Phenomenex Zebron ZB-5MSplus capillary column (30 m L × 0.25 mm ID × 1.0 μm df), using the methods previously developed[40]. Briefly, 1 μL of sample was injected onto the GC column for separation, with an injector temperature of 250 °C. The oven temperature was held at the initial temperature of 40 °C for 2 min before increasing to 150 °C at a rate of 4 °C/min. This was held for 4 min before increasing to 290 °C at a rate of 6 °C/min. This final temperature was held for 2 min. Mass spectra were acquired in positive ion mode from m/z 45–350 with no solvent delay. Quantitation of analytes was accomplished by creating an external standard curve ranging from 5 to 750 ppm (detection limit:5 ppm) using the area under the peak corresponding to the analyte. The resulting linear trendline was used to determine the concentration of the analyte in each sample. Clean air blanks were used as negative controls. The chromatograms were analyzed as follows: Library Match Factor was recorded for peaks in the test and blank samples that were attributable to specific compounds, and duplicate compounds that eluted closely were counted as one peak. The compounds found in blanks were considered as contaminants and removed. The compounds were then characterized based on knowledge-based networks using the Globally Harmonized System of Classification and Labeling of Chemicals (GHS) and MSDS.

Multispecies biofilm model. Artificial saliva was made following the Marshall Group Research protocol for artificial saliva[42]. SHI medium was prepared according to the protocol described by Tian et al.[43]. Biofilms were developed using the modifications[15] from the protocol established by Guggenheim et al.[44]. Briefly, sterilized, sintered hydroxyapatite (HA) disks (Clarkson Chromatography Products, South Williamsport, PA) were incubated in artificial saliva for 24 h to establish a pellicle coat, following which multispecies commensal primary biofilms were generated by seeding six pioneer species [*Streptococcus oralis* (ATCC 35037), *S. sanguis* (10556), *S. mitis* (49456), *Actinomyces naeslundii* (12104), *Neisseria mucosa* (25997), and *Veillonella parvula* (17745)] and incubating under aerobic conditions in a 1:1(v/v) mixture of SHI media and artificial saliva. Pathogen-rich biofilms were created by further seeding the commensal biofilms with an intermediate bridging colonizer [*Fusobacterium nucleatum* (10953), secondary biofilm] followed 24 h later by *Porphyromonas gingivalis* (33277), *Filifactor alocis* (35896), *Selenomonas sputigena* (35185), *S. noxia* (43541), *Campylobacter gracilis* (33236), *Prevotella intermedia* (25611), *Parvimonas micra* (33270), and *Tannerella forsythia* (43037) and incubating under anaerobic conditions for a further 24 h (tertiary biofilms). The biofilms were created at the same time and frozen at −80 °C to prevent batch effects. Prior to experimentation, biofilms were transferred to fresh medium for 24 h following the "revival" protocol established by Guggenheim et al.[45]. Biofilm viability was assessed using a BacLight kit (Life Technologies, NY, USA) according to the manufacturer's instructions. Briefly, the bacteria were incubated in 1.5 mL of 0.3% SYTO 9® and propidium iodide and the fluorescence measured at 486 and 520 nm using a Spectral FlowView confocal microscope at ×10 magnification. The ratio of green to red fluorescence was computed and used to determine bacterial viability.

ENDS exposure. Electronic cigarette vapor (ECV) was prepared following our previous protocol with minor modifications[10]: a moderate-sized e-cigarette pen was filled with either nicotine-free e-liquid or 6 mg/ml nicotine e-liquid, both unflavored, and actuated by pressing "on" for 5 s then "off" for 25 s and repeated for a total of 10 min or 20 "puffs". The e-cigarette was connected via Pasteur pipettes into 5 ml of artificial saliva. ECV was prepared immediately before each use. The nicotine-free and nicotine-containing ECV replaced the artificial saliva in the 50/50 saliva/SHI media incubating mixture following each comparative exposure condition. To maintain the consistency of ECV between experiments, an

optical density of 0.15 at 600 nm represented 100%. All experiments were performed in triplicate and repeated two times, giving rise to 6 datapoints per outcome.

Bacterial metabolomics. Following 'revival' of each respective biofilm, growth media was removed, and biofilms were exposed to 100% artificial saliva following each respective exposure condition: nicotine-free, nicotine-containing, and control conditions. Saliva supernatant was collected for 1-, 2-, 4-, and 8-hour timepoints. Samples were spun at 10,000 rpm and decanted to remove cell debris. Saliva was analyzed by nuclear magnetic resonance (NMR) spectroscopy to identify the timeline of peak metabolite generation. Trapped ion mobility spectrometry tandem time-of-flight (TIMS-TOF) was then used to identify metabolites generated following 1-h of e-cigarette exposure.

Nuclear magnetic resonance (NMR) spectroscopy. Untargeted one-dimensional (1D) 1H NMR of the bacterial supernatant was analyzed with 800 MHz spectrometer (Bruker, USA). Samples were analyzed using the first increment of NOESY pulse sequence with presaturation and the CPMG pulse sequence. 1H NMR spectra was acquired at 298 K using 128 scans and 64 K data points. 2D NMR was applied on selected samples to confirm the identity of the specific metabolites. Free induction decays (FIDs) were multiplied by a decaying exponential function with a 1 Hz line broadening factor prior to Fourier transformation. The 1H NMR spectra were corrected manually for phase and a polynomial fourth-order function applied for base-line correction in order to achieve accurate and reproducible measurements upon integration of the signals of interest. Chemical shifts were reported in ppm as referenced to TSP ($\delta = 0$). Spectra were processed and analyzed using Topspin 3.2. Prior to statistical data analysis, each bucketed region was normalized to the total sum of the spectral intensities.

TIMS-TOF data processing and metabolite annotations. Bacterial supernatant was collected following 1 h of exposure to e-cigarette and subjected to matrix-assisted laser desorption ionization–trapped ion mobility spectrometry time-of-flight mass spectrometry (TIMS-TOF) (Bruker, USA). The acquired raw datasets were initially processed by using SCiLS lab 2021a software (Bruker, USA). Mass range was selected between 20 and 2000 m/z for assigning regions. Files were then exported in Metaboscape 2021b (Bruker, USA) for annotations and further downstream analysis. After checking the regions, all m/z points were annotated by using eleven libraries from analyte list of libraries i.e HMDB library 2.0_KEGG, Lipids Human Brain metabolites library, Lipids Mouse Kidney metabolites library, Small Molecules metabolites library, N-Glycan human library, Cell culture nutrient library, Fatty acids library, HMDB plasma metabolites library, Lipid maps library, Natural products metabolites library and CCS compendium library. Also, annotations were carried out by using a range of Mass spectral libraries provided by Metaboscape like Bruker Sumner MetaboBASE plant library, Bruker NIST 2020 MSMS Spectral Library hr-2, MSDIAL- TandemMassSpectralAtlas libraries for both positive and negative ions. The parameters (tolerances and scoring) used for annotations are as follows m/z: 2.0–5.0 ppm, msigma 25–500 and CCS 2.0–5.0%. Annotations of metabolites against all Lipid classes available in Metaboscape was also carried out with the same m/z and mSigma values. The compounds were further characterized based on knowledge-based networks using the PubChem (https://pubchem.ncbi.nlm.nih.gov/) and Lotus databases (https://lotus.naturalproducts.net/).

Statistical analysis. Each reaction was run in triplicate, and the experiments duplicated generating 6 datapoints for every timepoint and biofilm type. Bucket tables from each experiment was exported from Metaboscape 2021b for further statistical data analysis in R. Nonmetric Dimensional scaling was carried out in R by using vegan package. In order to determine the statistical difference between the metabolites

concentration between groups, ANOSIM was employed. For heatmap generation p values (FDR) based on t-test between the two groups were also calculated and table was exported in R to further plot the heatmap between the top 50 most significantly different metabolites between the two comparison groups. Pheatmap library was used to plot the heatmap. After Peak intensity table was imported, the uploaded data was log-transformed, and normalization was done by mean subtraction. Other parameters included the use of the correlation-based clustering of the columns. Metaboanalyst (v6.0) was used to analyze the role of microbial community composition via PLSDA[46]. The ability of metabolites to discriminate between groups was examined using a machine-learning algorithm (RandomForest package in R). Two-thirds of the dataset was used to train the algorithm, which was tested on the remaining data. *Stratify = y* command was used to ensure that the train and test datasets comprised of samples from each group in the same proportions as the original dataset. This was iterated 10 times and the mean 'importance' computed for each marker. The robustness of the classifier was evaluated using ROC curves (ROCR package for R). For each iteration of the test, a 'confusion table' of the number of correctly classified and misclassified samples was used to compute sensitivity and specificity.

RNA isolation, metagenomic sequencing, and analysis. Biofilms were harvested following one hour of exposure to e-cigarettes and RNA isolated using the mirVana miRNA isolation kit (Applied Biosystems). Ribosomal RNA was depleted, and mRNA was enriched by modified capture hybridization approach (MICROBExpress mRNA enrichment kit, Thermo Fisher Scientific). Enriched mRNA served as a template for the polyadenylation reaction and complementary DNA synthesis. Microbial libraries were clustered on the Illumina HiSeq 4000 platform, and 150-bp paired-end sequencing was performed. The Illumina base-calling pipeline was used to process the raw fluorescence images and call sequences. Raw reads with >10% unknown nucleotides or with >50% low-quality nucleotides (quality value, <20) were discarded. Microbial transcripts were quality-filtered using Sickle v1.33 (default parameters) and aligned against the RefSeq nonredundant proteins database using DIAMOND v0.8.3.65[47]. Aligned sequences were annotated to the KEGG database using MEGAN 6[48]. COGs that did not exceed a relative abundance of 0.01% were excluded from analysis as an unsupervised feature reduction technique.

Quality control. All samples were sequenced in two runs; and to minimize batch effects, samples were randomly assigned to each run. Replicate sequencing was carried out for two samples in each batch, and the replicates showed good reliability across the five batches, with coefficient of variability (SD/mean) ranging from 3.4 to 5.1% for predominant functions (carbohydrate metabolism, respiration, and virulence, disease, and defense).

Network analysis. Co-occurrence networks were created between abundances of functionally annotated transcripts and metabolites for each group. JMP (SAS Institute Inc., Cary, NC, USA) was used to calculate pairwise correlations; significant co-occurrences (defined as Spearman's rho >0.75 and $p < 0.05$ (t- test of rho)) were imported into Networkx[49] to create the graph structures, and Gephi[50] to visualize and label the graphs. Betweenness centrality was calculated using Python package 'Networkx'. Robustness of clustering was examined using an algorithm incorporating betweenness centrality, differential abundances, and frequency of occurrence in a group as described before[51]. Network anchors were identified by an algorithm incorporating betweenness centrality and frequency of occurrence in a group. Betweenness centrality was calculated using Python package "*Networkx*" and transcripts were ranked based on this metric. For each group, metabolites and transcripts that were present in at least 75% of the samples were identified as the "core". Metabolites or transcripts that demonstrated a high betweenness centrality (top 20% in each network), and were part of the group's core were identified as network anchors.

Biofilm imaging. To enable confocal microscopic imaging, we stained the biofilms using the BacLight kit (Life Technologies, NY) according to the manufacturer's instructions. Briefly, the biofilms were incubated in 1.5 ml of 0.3% SYTO 9 and propidium iodide, and the fluorescence was measured at 486 and 520 nm using a Spectral FlowView confocal microscope at 10× magnification. The ratio of green to red fluorescence was computed, and Z-stack images were obtained. A minimum of eight images per specimen was obtained to generate volume and area graphs. Total surface area and volume were determined using Imaris v9 (http://bitplane.com) from the constructed three-dimensional images. Boxplot comparisons of areas and volumes were visualized using Seaborn v0.9.0, and the significance of pairwise differences was determined using Tukey's post hoc test (JMP statistical software v13.0).

Clinical correlation. Clinical samples were collected in a previously published study[10]. We obtained approval for this study from the Office of Responsible Research Practices at The Ohio State University [IRB (Institutional Review Board) protocol number 2014H0062 and e-IBC protocol number 2015R00000005], and the study was conducted in accordance with approved guidelines. We recruited 123 systemically [ASA I (American Society of Anesthesiologists Physical Status Classification I)] and periodontally healthy individuals [attachment loss ≤1; less than three sites with 4 mm of probe depths (PD); bleeding index (BOP) ≤ 20%] following informed consent and clinical and radiographic examination to each of five groups: (i) smokers (25), (ii) nonsmokers (25), (iii) e-cigarette users (20), (iv) former smokers currently using e-cigarettes (25), and (v) concomitant cigarette and e-cigarette users (28). Current smokers were those who had at least a five pack-year history and had no prior history of e-cigarette use. Never smokers were those who had smoked less than 100 cigarettes in their lifetime and none in the past year, and e-cigarette users were those who used e-cigarettes daily for at least 3 months, with at least one cartridge per day or 1 ml of liquid per day. Former smokers were those who had quit smoking for at least 1 year. Exclusion criteria for all groups included controlled or uncontrolled diabetes, HIV infection, use of immunosuppressant medications, bisphosphonates, or steroids, antibiotic therapy or oral prophylactic procedures within the preceding 3 months, and fewer than 20 teeth in the dentition. Saliva was collected from each participant and analyzed via TIMS-TOF.

Data availability
All data generated or analyzed during this study are included in this published article and its supplementary information files.

References
1. Wild, C. P. Complementing the Genome with an "Exposome": the outstanding challenge of environmental exposure measurement in molecular epidemiology. *Cancer Epidemiol. Biomark. Prev.* **14**, 1847–1850 (2005).
2. Wild, C. P. The exposome: from concept to utility. *Int. J. Epidemiol.* **41**, 24–32 (2012).
3. Wang, T. W. et al. E-cigarette use among middle and high school students - United States, 2020. *Mmwr Morb. Mortal. W* **69**, 1310–1312 (2020).
4. Ali, F. R. M. et al. E-cigarette unit sales by product and flavor type, and top-selling brands, United States, 2020-2022. *Mmwr Morb. Mortal. W* **72**, 672–677 (2023).
5. Cooper, M. et al. E-cigarette use among middle and high school students - United States, 2022. *Mmwr Morb. Mortal. W* **71**, 1283–1285 (2022).
6. St. Helen, G. & Eaton, D. L. Public health consequences of e-Cigarette Use. *JAMA Intern. Med.* **178**, 984–986 (2018).

7. Marques, P., Piqueras, L. & Sanz, M.-J. An updated overview of e-cigarette impact on human health. *Respir. Res.* **22**, 151 (2021).

8. Assiri, M. A. et al. Electronic cigarette vapor disrupts key metabolic pathways in human lung epithelial cells. *Saudi Pharm. J.* **32**, 101897 (2024).

9. Wang, Q., Ji, X. & Rahman, I. Dysregulated metabolites serve as novel biomarkers for metabolic diseases caused by E-Cigarette vaping and cigarette smoking. Metabolites 11. https://doi.org/10.3390/metabo11060345 (2021).

10. Ganesan, S. M. et al. Adverse effects of electronic cigarettes on the disease-naive oral microbiome. *Sci. Adv.* **6**, eaaz0108 (2020).

11. Pushalkar, S. et al. Electronic cigarette aerosol modulates the oral microbiome and increases risk of infection. *iScience* **23**, 100884 (2020).

12. Thomas, S. C. et al. Electronic cigarette use promotes a unique periodontal microbiome. *mBio* **13**, e0007522 (2022).

13. Yang, I., Rodriguez, J., Young Wright, C. & Hu, Y.-J. Oral microbiome of electronic cigarette users: a cross-sectional exploration. *Oral. Dis.* **29**, 1875–1884 (2023).

14. Postler, T. S. & Ghosh, S. Understanding the Holobiont: how microbial metabolites affect human health and shape the immune system. *Cell Metab.* **26**, 110–130 (2017).

15. Shah, S. A. et al. The making of a miscreant: tobacco smoke and the creation of pathogen-rich biofilms. *NPJ Biofilms Microbiomes* **3**, 26 (2017).

16. Kumar, P. S. Smoking and the subgingival ecosystem: a pathogen-enriched community. *Future Microbiol.* **7**, 917–919 (2012).

17. Kumar, P. S., Griffen, A. L., Moeschberger, M. L., Leys, E. J. Identification of candidate periodontal pathogens and benficial species using quantitative 16S clonal analysis. *J. Clin. Microbiol.* **43**, 3944–3955 (2005).

18. Wishart, D. S. et al. HMDB 5.0: the Human Metabolome Database for 2022. *Nucleic Acids Res.* **50**, D622–D631 (2022).

19. Bagaitkar, J. et al. Tobacco-induced alterations to Porphyromonas gingivalis-host interactions. *Environ. Microbiol.* **11**, 1242–1253 (2009).

20. Ertel, A., Eng, R. & Smith, S. M. The differential effect of cigarette smoke on the growth of bacteria found in humans. *Chest* **100**, 628–630 (1991).

21. Huang, R., Li, M. & Gregory, R. L. Effect of nicotine on growth and metabolism of Streptococcus mutans. *Eur. J. Oral. Sci.* **120**, 319–325 (2012).

22. Kolenbrander, P. E. Oral microbial communities: biofilms, interactions, and genetic systems. Ann. Rev. Microbiol. 54. https://doi.org/10.1146/annurev.micro.54.1.413 (2000).

23. Kolenbrander, P. E., Andersen, R. N. & Moore, L. V. Coaggregation of Fusobacterium nucleatum, Selenomonas flueggei, Selenomonas infelix, Selenomonas noxia, and Selenomonas sputigena with strains from 11 genera of oral bacteria. *Infect. Immun.* **57**, 3194–3203 (1989).

24. Abou Diwan, M. et al. Impact of pesticide residues on the gut-microbiota–blood–brain barrier axis: a narrative review. *Int. J. Mol. Sci.* **24**, 6147 (2023).

25. Djekkoun, N., Lalau, J.-D., Bach, V., Depeint, F. & Khorsi-Cauet, H. Chronic oral exposure to pesticides and their consequences on metabolic regulation: role of the microbiota. *Eur. J. Nutr.* **60**, 4131–4149 (2021).

26. Joly Condette, C. et al. Use of molecular typing to investigate bacterial translocation from the intestinal tract of chlorpyrifos-exposed rats. *Gut Pathog.* **8**, 1–12 (2016).

27. Park, B. et al. The mediating roles of the oral microbiome in saliva and subgingival sites between e-cigarette smoking and gingival inflammation. *BMC Microbiol.* **23**, 35 (2023).

28. Xu, F. et al. Comparative effects of E-cigarette aerosol on periodontium of periodontitis patients. Front. Oral Health 2. https://doi.org/10.3389/froh.2021.729144 (2021).

29. Tang, H. et al. Regulation of nicotine tolerance by quorum sensing and high efficiency of quorum quenching under nicotine stress in Pseudomonas aeruginosa PAO1. *Front. Cell Infect. Microbiol.* **8**, 88 (2018).

30. Reichhardt, C. & Parsek, M. R. Confocal laser scanning microscopy for analysis of pseudomonas aeruginosa biofilm architecture and matrix localization. Front. Microbiol. 10. https://doi.org/10.3389/fmicb.2019.00677 (2019).

31. Catala-Valentin, A. et al. E-Cigarette aerosol exposure favors the growth and colonization of oral streptococcus mutans compared to commensal streptococci. *Microbiol. Spectr.* **10**, e0242121 (2022).

32. García-Contreras, R. et al. Quorum sensing enhancement of the stress response promotes resistance to quorum quenching and prevents social cheating. *Isme J.* **9**, 115–125 (2015).

33. Özkaya, Ö., Xavier, K. B., Dionisio, F. & Balbontín, R. Maintenance of microbial cooperation mediated by public goods in single- and multiple-trait scenarios. J. Bacteriol. 199. https://doi.org/10.1128/jb.00297-17 (2017).

34. Irusa, K. F., Finkelman, M., Magnuson, B., Donovan, T. & Eisen, S. E. A comparison of the caries risk between patients who use vapes or electronic cigarettes and those who do not: a cross-sectional study. *J. Am. Dent. Assoc.* **153**, 1179–1183 (2022).

35. Vemulapalli, A., Mandapati, S. R., Kotha, A. & Aryal, S. Association between vaping and untreated caries: a cross-sectional study of National Health and Nutrition Examination Survey 2017-2018 data. *J. Am. Dent. Assoc.* **152**, 720–729 (2021).

36. Irusa, K. F., Vence, B. & Donovan, T. Potential oral health effects of e-cigarettes and vaping: a review and case reports. *J. Esthet. Restor. Dent.* **32**, 260–264 (2020).

37. Schuster, M., Sexton, D. J. & Hense, B. A. Why quorum sensing controls private goods. Front. Microbiol. 8. https://doi.org/10.3389/fmicb.2017.00885 (2017).

38. Laura, E. C. A., Shymaa, E. & Elisa, M. *Frontiers in Staphylococcus aureus* (eds Enany Shymaa & E. Crotty Alexander L.) Ch. 4 (IntechOpen, 2017).

39. Martínez-Solís, E. A. et al. Comparison of the phenotypic profile of antimicrobial resistance in the oral microbiota of non-smokers, tobacco smokers, and electronic cigarette vapers-a pilot study. *Proc. Sci. Res. Univ. Anáhuac. Multidiscip. J. Healthc.* **1**, 5–13 (2021).

40. Kim, J. J. et al. Universal electronic-cigarette test: physiochemical characterization of reference e-liquid. *Tob. Induc. Dis.* **15**, 14 (2017).

41. Behar, R. Z., Hua, M. & Talbot, P. Puffing topography and nicotine intake of electronic cigarette users. *PLoS ONE* **10**, e0117222 (2015).

42. Saeki, K., Marshall, G. W., Gansky, S. A., Parkinson, C. R. & Marshall, S. J. Strontium effects on root dentin tubule occlusion and nanomechanical properties. *Dent. Mater.* **32**, 240–251 (2016).

43. Tian, Y. et al. Using DGGE profiling to develop a novel culture medium suitable for oral microbial communities. *Mol. Oral. Microbiol.* **25**, 357–367 (2010).

44. Guggenheim, B. et al. In vitromodeling of host-parasite interactions: the 'subgingival' biofilm challenge of primary human epithelial cells. *BMC Microbiol.* **9**, 280 (2009).

45. Guggenheim, B. et al. In vitro modeling of host-parasite interactions: the 'subgingival' biofilm challenge of primary human epithelial cells. *BMC Microbiol.* **9**, 280 (2009).

46. Chong, J. & Xia, J. MetaboAnalystR: an R package for flexible and reproducible analysis of metabolomics data. *Bioinformatics* **34**, 4313–4314 (2018).

47. Buchfink, B., Xie, C. & Huson, D. H. Fast and sensitive protein alignment using DIAMOND. *Nat. Methods* **12**, 59–60 (2015).

48. Huson, D. H., Auch, A. F., Qi, J. & Schuster, S. C. MEGAN analysis of metagenomic data. *Genome Res.* **17**, 377–386 (2007).

49. Hagberg, A. A., Schult, D. A. & Swart, P. J. Exploring network structure, dynamics, and function using NetworkX. *Proc. 7th Python Sci. Conf.* **2008**, 11–16 (2008).

50. Bastian, M., Heymann, S. & Jacomy, M. Gephi: an open source software for exploring and manipulating networks. *ICWSM* **8**, 361–362 (2009).

51. Paropkari, A. D., Leblebicioglu, B., Christian, L. M. & Kumar, P. S. Smoking, pregnancy and the subgingival microbiome. *Sci. Rep.* **6**, 30388 (2016).

Competing interests
The authors declare no competing interests.

Additional information
Supplementary information The online version contains supplementary material available at https://doi.org/10.1038/s41522-025-00709-7.

Correspondence and requests for materials should be addressed to Purnima S. Kumar.

Reprints and permissions information is available at http://www.nature.com/reprints

Publisher's note Springer Nature remains neutral with regard to jurisdictional claims in published maps and institutional affiliations.